ISSN 1674-1056
http://cpb.iphy.ac.cn
http://iopscience.iop.org/cpb
中国物理 B
Chinese Physics
中国物理 Chinese Physics B

Evolution of helium bubbles in nickel-based alloy by post-implantation annealing

Rui Zhu(朱睿), Qin Zhou(周钦), Li Shi(史力), Li-Bin Sun(孙立斌), Xin-Xin Wu(吴莘馨), Sha-Sha Lv(吕沙沙), and Zheng-Cao Li(李正操)

Citation: Chin. Phys. B, 2021, 30 (**8**): 086102. DOI: 10.1088/1674-1056/ac0783
Journal homepage: http://cpb.iphy.ac.cn; http://iopscience.iop.org/cpb

What follows is a list of articles you may be interested in

In-situ TEM observation of the evolution of helium bubbles in Mo during He^+ irradiation and post-irradiation annealing

Yi-Peng Li(李奕鹏), Guang Ran(冉广), Xin-Yi Liu(刘歆翌), Xi Qiu(邱玺), Qing Han(韩晴), Wen-Jie Li(李文杰), and Yi-Jia Guo(郭熠佳)
Chin. Phys. B, 2021, 30 (**8**): 086109. DOI: 10.1088/1674-1056/abff48

Effect of helium concentration on irradiation damage of Fe-ion irradiated SIMP steel at 300 ℃ and 450 ℃

Zhen Yang(杨振), Junyuan Yang(杨浚源), Qing Liao(廖庆), Shuai Xu(徐帅), and Bingsheng Li(李炳生)
Chin. Phys. B, 2021, 30 (**5**): 056107. DOI: 10.1088/1674-1056/abd6f9

Comparison of helium bubble formation in F82H, ODS, SIMP and T91 steels irradiated by Fe and He ions simultaneously

Bingsheng Li(李炳生), Zhen Yang(杨振), Shuai Xu(徐帅), Kongfang Wei (魏孔芳), Zhiguang Wang(王志光), Tielong Shen(申铁龙), Tongmin Zhang(张桐民), and Qing Liao(廖庆)
Chin. Phys. B, 2021, 30 (**3**): 036102. DOI: 10.1088/1674-1056/abc2b4

Extended damage range of $(Al_{0.3}Cr_{0.2}Fe_{0.2}Ni_{0.3})_3O_4$ high entropy oxide films induced by surface irradiation

Jian-Cong Zhang(张健聪), Sen Sun(孙森), Zhao-Ming Yang(杨朝明), Nan Qiu(裘南), Yuan Wang(汪渊)
Chin. Phys. B, 2020, 29 (**6**): 066104. DOI: 10.1088/1674-1056/ab8374

Effect of microstructure on ^3He migration in $TiT_{1.9}$ films

Haifeng Wang(王海峰), Shuming Peng(彭述明), Wei Ding(丁伟), Huahai Shen(申华海), Weidu Wang(王维笃), Xiaosong Zhou(周晓松), Xinggui Long(龙兴贵)
Chin. Phys. B, 2018, 27 (**9**): 096103. DOI: 10.1088/1674-1056/27/9/096103

SPECIAL TOPIC — Ion beam modification of materials and applications

Evolution of helium bubbles in nickel-based alloy by post-implantation annealing*

Rui Zhu(朱睿)[1,2], Qin Zhou(周钦)[1,†], Li Shi(史力)[1], Li-Bin Sun(孙立斌)[1], Xin-Xin Wu(吴莘馨)[1], Sha-Sha Lv(吕沙沙)[3,‡], and Zheng-Cao Li(李正操)[2]

[1] *Institute of Nuclear and New Energy Technology, Tsinghua University, Beijing* 100084, *China*
[2] *Key Laboratory of Advanced Materials (Ministry of Education), School of Materials Science and Engineering, Tsinghua University, Beijing* 100084, *China*
[3] *Key Laboratory of Beam Technology, Ministry of Education, College of Nuclear Science and Technology, Beijing Normal University, Beijing* 100875, *China*

(Received 13 January 2021; revised manuscript received 31 March 2021; accepted manuscript online 3 June 2021)

Nickel-based alloys have been considered as candidate structural materials used in generation IV nuclear reactors serving at high temperatures. In the present study, alloy 617 was irradiated with 180-keV helium ions to a fluence of 3.6×10^{17} ions/cm^2 at room temperature. Throughout the cross-section transmission electron microscopy (TEM) image, numerous over-pressurized helium bubbles in spherical shape are observed with the actual concentration profile a little deeper than the SRIM predicted result. Post-implantation annealing was conducted at 700 °C for 2 h to investigate the bubble evolution. The long-range migration of helium bubbles occurred during the annealing process, which makes the bubbles of the peak region transform into a faceted shape as well. Then the coarsening mechanism of helium bubbles at different depths is discussed and related to the migration and coalescence (MC) mechanism. With the diffusion of nickel atoms slowed down by the alloy elements, the migration and coalescence of bubbles are suppressed in alloy 617, leading to a better helium irradiation resistance.

Keywords: helium bubble, coarsening mechanism, nickel-based alloy

PACS: 61.72.U–, 61.80.Jh, 61.82.–d **DOI:** 10.1088/1674-1056/ac0783

1. Introduction

Generation IV nuclear power plants are supposed to deliver significant improvements compared with current generation III reactor systems in the aspects of sustainability, safety, economics, and proliferation resistance.[1] To utilize nuclear energy in a more economic way, the normal operating temperature of generation IV systems usually is higher than current reactors. The core outlet temperature of the very high temperature reactor (VHTR) and the molten salt reactor (MSR) exceed 700 °C for high power generation efficiency and hydrogen production.[2,3] The structural materials and components in these reactors are required to be reliable in such a high temperature for long service life.

Due to its good creep property and stability at high temperatures, alloy 617 has been considered as candidate structural materials serving at a temperature above 700 °C in generation IV nuclear reactors.[4] Alloy 617 is a nickel-based alloy with a high content of cobalt (Co), chromium (Cr), and molybdenum (Mo), which possesses great creep strength and corrosion resistance at high temperatures.[5] However, structural materials used in reactors are undergoing radiation damage which could result in severe performance degradation. The damage of materials exposed to neutron irradiation has two different types: defects and element transmutation. First, irradiation of energetic particles in the lattice of material produces atomic displacements, resulting in many interstitials and vacancies. The number of interstitials and vacancies is equal, forming the Frenkel pairs. The remaining interstitials and vacancies further evolve into different defects such as clusters, dislocation loops, voids,[6] *etc*. Also, nuclear reactions introduce foreign elements in the lattice. For nickel-based alloy, abundant helium atoms can easily be introduced into the lattice for a high (n, α) reaction cross section. Because of its low solubility, helium atoms precipitate into bubbles and deteriorate the mechanical properties of materials, especially at high temperatures.[7–9] Hence, it is necessary to investigate the helium behavior of the nickel-based alloy.

There are two commonly used experimental methods to analyze their irradiation resistance. One method is that specimens are implanted directly at high temperatures and the other is where helium atoms are implanted at room temperature and subsequently annealed isochronally at high temperatures.[10] During the high-temperature irradiation process, the implanted helium atoms will be trapped by the previously nucleated helium bubbles, so they tend to be immovable. The evolving bubbles preserve information about the nucleation process.[11] For the second method, the initially formed helium–vacancy clusters migrate and coarsen to a bubble during the annealing

*Project supported by the Special Funds for the Key Research and Development Program of the Ministry of Science and Technology of China (Grant Nos. 2017YFB0702201 and 2020YFB1901800) and the National Natural Science Foundation of China (Grant Nos. 11975135 and 12005017).

†Corresponding author. E-mail: qinzhou@tsinghua.edu.cn
‡Corresponding author. E-mail: lvss@bnu.edu.cn

© 2021 Chinese Physical Society and IOP Publishing Ltd

process, providing information on helium diffusion or bubbles migration.

Based on post-implantation annealing, Carsughi *et al.* found that the helium bubbles were in bimodal size distribution and the coarsening mechanism of bubbles in the interior and grain boundaries is different.[12] Villacampa *et al.* conducted the helium implantation at 300 °C and then annealed from 650 °C to 1000 °C, the results suggest that bubbles grew by the coarsening mechanism in both cases.[13] The coarsening mechanism has important effects on the size and number density of helium bubbles which determine the mechanical properties of the material under helium implantation. Recently, the evolution of helium bubbles in a pre-helium irradiated FeCrAl alloy during high-temperature annealing was investigated by *in-situ* transmission electron microscopy (TEM), and it was found that two bubbles merged into one large-sized bubble, supporting the migration and coalescence mechanism.[14] Nevertheless, the helium behavior of nickel-base alloys at high temperatures is still not fully understood.

In the present study, the evolution of helium bubbles in alloy 617 has been investigated by helium implantation and high-temperature annealing. The morphology, size, and distribution of helium bubbles were studied by TEM observation, then we discussed the corresponding coarsening mechanism with different depths and crystalline parts to analyze its irradiation resistance.

2. Experimental procedure

The chemical composition of alloy 617 is shown in Table 1. The rod samples were cut into the square plate of 10 mm×10 mm ×1 mm (thickness) by wire-electrode cutting. The surface of all the samples was mechanically polished with silicon carbide paper of different grits and diamond spray. Finally, the samples were ultrasonically cleaned with acetone for 30 minutes. The helium implantation experiments were conducted at Beijing Normal University. All the samples were irradiated with 180-keV helium ions to a fluence of 3.6×10^{17} ions/cm^2 at room temperature. The irradiated samples were annealed at 973 K for 2 hours in a vacuum (below 1×10^{-5} Pa). The helium ion distribution and irradiation damage were simulated by SRIM 2013 program with the Kinchin–Pease quick calculation mode.[15] Detailed simulation and irradiation process are available in Ref. [16]. Figure 1 shows the displacement per atom (dpa) results and the helium concentration profile calculated by SRIM. The fluence of 3.6×10^{17} ions/cm^2 corresponds to the peak dose was 10 dpa and the maximum helium concentration was 22 at.%.

Table 1. Chemical composition of alloy 617 (in units of wt%).

Elements	Ni	Cr	Co	Mo	Fe	Mn	Si	Al	Ti	C	S
Content	≥ 44.5	20.0–24.0	10–15	8.0–10.0	≤ 3	1.00	1.00	0.8–1.5	≤ 0.6	0.05–0.15	0.02

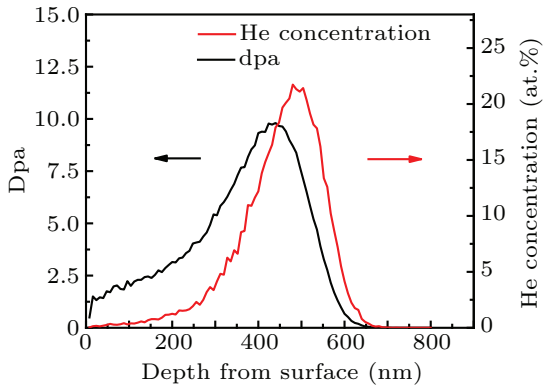


Fig. 1. SRIM simulation of the dpa and helium concentration profiles induced by 180-keV helium implantation.

The cross-section TEM sample was prepared by the lift-out technique using a focused-ion beam (FIB). The thickness of the samples was approximately 50 nm. Figure 2 shows the front view of the finished samples. The surface of the sample was coated with a layer of platinum to prevent the damage from Ga ion beam. A plasma cleaner was employed to remove the potential carbon contamination on the surface. Two small holes in the irradiation layer were formed during the thinning process. Due to the presence of helium bubbles, this area is more fragile and the Ga ion beam penetrates the sample during the thinning process. The irradiation-induced changes of microstructure were characterized using a JEM-2100F TEM operated at 200 kV with a point resolution of 0.23 nm.

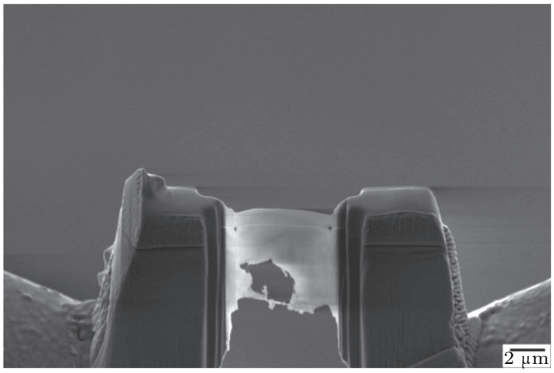


Fig. 2. The front view of the finished sample using an FIB.

3. Results and discussion

3.1. Helium irradiation at room temperature

Figure 3 shows the cross-section TEM bright-field image of the irradiated specimen at room temperature. The corresponding damage and helium concentration depth profile simulated by SRIM are superimposed with the TEM image. The

direction indicated by the blue arrow is the incident direction of helium ions, the depth of 0 at the horizontal coordinate-axis indicates the sample surface. Many defects in spherical shape are observed throughout the TEM image. These defects have been identified as helium bubbles by conducting the TEM from over-focus to under-focus. It can be seen from Fig. 3(a) that high-density and large-sized helium bubbles can be observed in the range of 400 nm–700 nm from the surface, showing a "helium bubble band" with a width of 300 nm. According to the size and number density of helium bubbles in this area, it can be further divided into 3 sub-regions, namely, "region A", "region B", and "region C". The TEM images of these three sub-regions are shown in Figs. 4(a)–4(c). In addition to this helium bubble band, there are also many helium bubbles near the surface. The distribution of helium bubbles at the range of 100 nm–200 nm from the surface is shown in Fig. 4(d). However, no "black dots" and dislocation loops are observed.

The size of helium bubbles near the surface is less than 1 nm, and the number density is about 1.25×10^{24} cm^{-2}. The number densities of helium bubbles with calculation in the three regions A, B, and C are 1.02×10^{24} cm^{-2}, 1.98×10^{24} cm^{-2}, and 2.75×10^{24} cm^{-2}, respectively. The average size of helium bubbles is 3.4 nm, 2.6 nm, and 1.9 nm, respectively. From the irradiated surface to 400 nm, the number density and size of helium bubbles increase with the depth, and the peak of number density is reached in the "region C" (the edge of helium bubble band). The helium bubble band is centered on "region A", and the average number density and size of helium bubbles are symmetrically distributed on both sides of "region A". The number density of helium bubbles drops sharply at a depth deeper than 700 nm, and no helium bubbles can be observed at 800 nm. The helium bubble concentration peak position simulated by SRIM is at 500 nm, which has not yet reached the center of the helium bubble band (550 nm). Therefore, the experimental result is about 50-nm deeper than the simulated result.

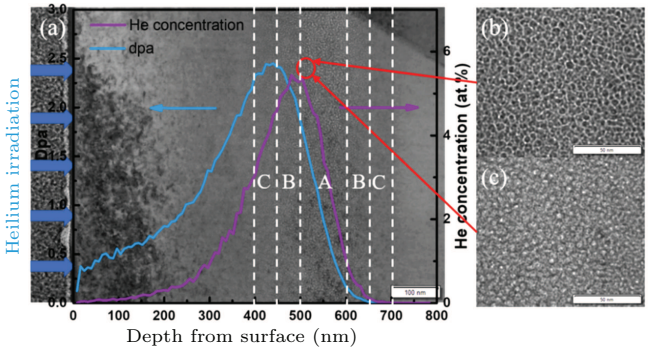


Fig. 3. (a) Bright-field TEM micrograph of the cross-section TEM sample implanted by helium at room temperature; (b) over-focus image of the circled area; (c) under-focus image of the circled area.

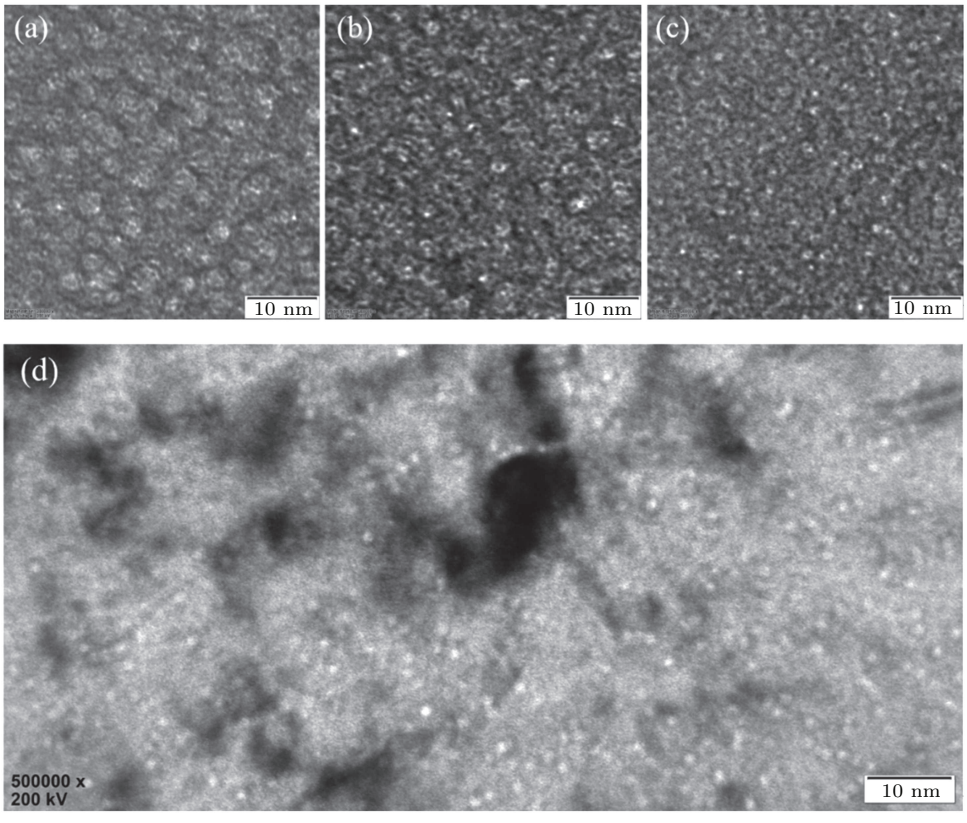


Fig. 4. Bright-field TEM micrograph of helium bubbles at (a) region A, (b) region B, (c) region C, and (d) the range of 100 nm–200 nm from surface.

The calculation of SRIM calculated that the cascade occurs in an amorphous solid and the channeling effect has been ignored. For the case of crystal implanted with light ions such as He, the channeling effect should be considered and the actual concentration profile shifts to a deeper place in the matrix. A shift of 5% of damage profile induced by channeling effect has been observed in helium implanted $SrTiO_3$.[17] It is worth noting that a considerable number of helium bubbles are observed within 100 nm from the surface. The size of these helium bubbles is below 1 nm.

According to the simulation results of SRIM, the helium concentration is lower than 0.3 at.% within 100 nm from the surface. Although the helium concentration in this area is very low, the damage distribution calculated by SRIM shows that the radiation damage is 0.5 dpa at 50 nm, which means the vacancy concentration is high near the surface. The vacancies induced by irradiation have a strong trapping effect on the incident helium atoms. The helium atoms trapped by vacancies are nucleated and grown to become the helium bubbles that can be observed by TEM.

3.2. Post-implantation annealing

Figure 5 shows the cross-section TEM observation of as-irradiated sample annealed at 700 °C for 2 h. Numerous helium bubbles in spherical or faceted shapes are observed throughout the TEM image. It can be seen from Fig. 5 that many helium bubbles with a size of more than 10 nm can be observed at 550 nm–700 nm from the surface. The center of the helium bubble band formed by room temperature irradiation is about 550 nm, and the center of the helium bubble band in the post-implantation annealing sample is about 600 nm, indicating the long-range migration of helium bubbles occurred during the annealing process.

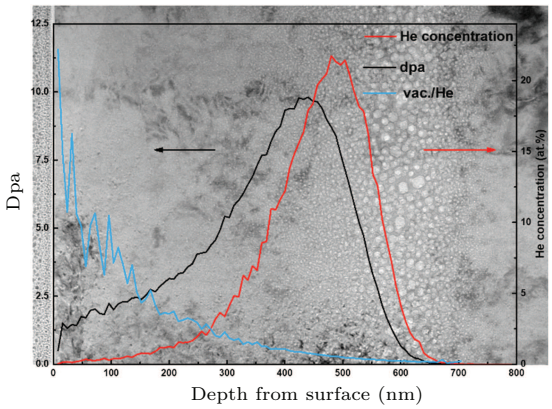


Fig. 5. Bright-field TEM micrograph of the cross-section TEM sample implanted by helium subsequently annealed at 700 °C for 2 h.

As shown in Figs. 6(a)–6(h), the helium bubbles are spherical in shape at a depth less than 400 nm or deeper than 750 nm. However, the helium bubbles are faceted in shape at a depth of 400 nm–750 nm. Despite the difference in the size of helium bubbles, all the bubbles are faceted in shape with the same preferential orientations, corresponding with the close packed planes of the host lattice.

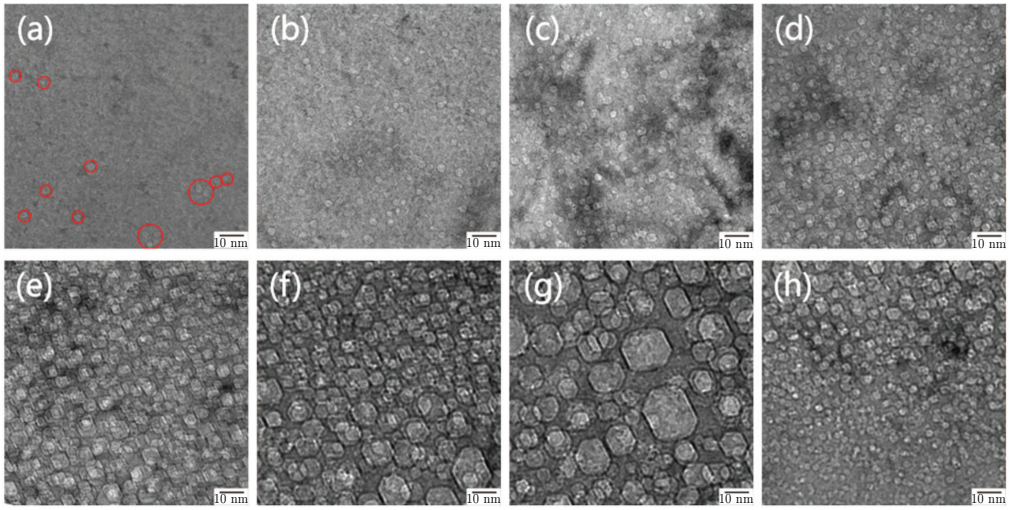


Fig. 6. The HRTEM images of annealed samples in different depths of alloy 617: (a) 0 nm–100 nm, (b) 100 nm–200 nm, (c) 200 nm–300 nm, (d) 300 nm–400 nm, (e) 400 nm–500 nm, (f) 500 nm–600 nm, (g) 600 nm–700 nm, and (h) 700 nm–800 nm.

Figure 7 shows the average size and number density of helium bubbles in each 50-nm width sub-region. The average size is the same near the surface region, whereas, the number densities vary greatly. The ratio of vacancy to helium decreases rapidly with increasing depth. The bubbles near the surface have enough vacancies to relax and reach the thermal equilibrium, resulting in the same size. However, the number density of bubbles depends on the helium concentration injected into the material. Vacancies induced by irradiation may be trapped by helium atoms to form He–vacancy clusters, serving as nucleation sites for helium bubbles. These existing bubbles tend to coarsen during the high-temperature annealing process, that is, their average size increases while the number density decreases.

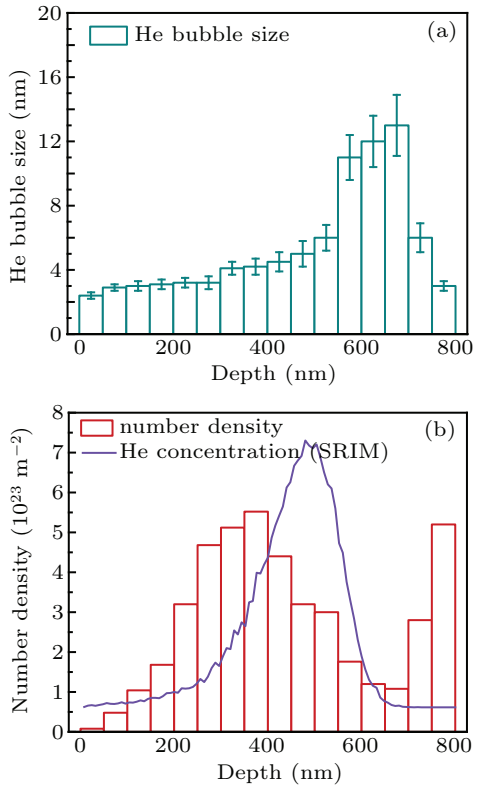


Fig. 7. The average He bubbles size (a) and number densities (b) at different depths of implanted samples annealed at 700 °C for 2 h.

3.3. Helium bubble coarsening mechanism

For the sample implanted at room temperature, the helium concentration at the peak position is about 22.5 at.%, the corresponding pressure should reach the mechanical stability limit in nickel, as high as 18 GPa.[7] However, for the post-implantation annealing sample, the pressure of helium bubbles is various in different areas. The ratio of helium atoms to vacancies is low near the surface, so there are enough vacancies for helium bubbles to absorb and establish thermal equilibrium. While the ratio of helium atoms to vacancies is high and the vacancy concentration is low in the bulk.

For the over-pressurized bubbles at a depth of 400 nm–750 nm, the pressure of bubbles cannot balance the surface tension force, that is, $P > 2\gamma/r$, where γ is the surface free energy. Thus, the extra elastic strain energy should be stored in the lattice. However, it is the total free energy of the system rather than the elastic strain energy that determines the shape of the bubble.[18] An analysis of experimental data on helium bubble coarsening in nickel together with theoretical calculation confirmed that the bubbles in the bulk can retain a considerable overpressure up to annealing temperatures higher than 1200 K ($\approx 0.7T_m$, T_m is the melting point).[19–21]

Consider a bubble of volume $V_0 = a^3$ and surface area $A = 6a^2 s$, where s is the shape parameter (for a cube, $s = 1$; for a sphere, $s < 1$; for a less regular shape, $s > 1$). After considering all the contributions to the system free energy, the following equation can be derived:[18,22]

$$\frac{\mathrm{d}(E_\mathrm{T})}{\mathrm{d}(s\gamma)} = V_0\left[\frac{6}{a} + \frac{4}{aK}\left(P - \frac{4s\gamma}{a}\right)\right], \tag{1}$$

where E_T is the total free energy of the system, K is the volume and bulk modulus of the bubble, respectively. The term $4s\gamma/a$ represents the pressure from surface tension force (for a sphere, $4s\gamma/a = 2\gamma/r$). For an over-pressurized bubble, equation (1) is positive. The value of $s\gamma$ is required to be as small as possible to minimize the system energy. Consequently, low-energy facets are preferentially developed in preference to a spherical shape that has higher surface energy.

There are two generally recognized mechanisms for the coarsening of helium bubbles: (i) bubble migration and coalescence (MC), and (ii) Ostwald ripening (OR).[7] MC means that bubbles migrate through surface diffusion and grow by coalescence with each other. OR means that large bubbles grow by absorbing helium atoms from the dissociation of small bubbles. In general, MC and OR dominate at relatively low and high temperatures (or high and low He concentrations), respectively.[7] Chernikov *et al.* reported that the coarsening mechanism of bubbles near the surface is OR whereas the coarsening mechanism of bubbles in the bulk is identified as MC during annealing between 973 K and 1273 K for helium-implanted nickel.[19] The discrepancy is attributed to the difference in vacancy concentration between the surface and bulk regions. Gao *et al.* also found this phenomenon in a nickel-based alloy, Hastelloy N, by post-irradiation annealing at 600 °C for 1 h and further annealed at 850 °C for 5 h.[23]

However, in the present study, the average size of bubbles near the surface is less than 3 nm, suggesting that the OR mechanism is not triggered. OR mechanism depends on the dissociation energy of helium atoms and vacancies, which is expected to be dominant at temperatures above $0.55T_m$.[21] For alloy 617, the annealing temperature should be higher than 750 °C. As shown in Fig. 4(d), the number density of the helium bubble is still very high at 100 nm–200 nm from the surface, high helium concentration also suppresses the trigger of the OR mechanism. Hence, it is assumed that coarsened helium bubbles near-surface are explained by the MC mechanism.

The high pressure of helium bubbles at a depth of 400 nm–750 nm effectively inhibits the triggering of the OR mechanism, reducing the coarsening rate.[19] As mentioned above, the helium bubble band migrated to the bulk by about 50 nm after annealing, indicating that the long-range migration of the small-sized helium bubble during the annealing process.

According to Fick's law of diffusion, helium atoms diffuse from a high-concentration area to a low-concentration area. There are still many helium bubbles on the side near the surface of the helium bubble band, which suppresses the diffusion of the helium bubble band to the surface. However, there

are no helium bubbles or even helium atoms at a depth deeper than 700 nm, so the helium bubble band migrated to the bulk. During the migration process, when the surfaces of two helium bubbles are in contact, they will coalesce into one helium bubble with a larger size. Therefore, in the present study, the coarsening mechanism of helium bubbles in different regions should be the migration and consolidation mechanism.

Yan *et al.* reported that big cavities with a size larger than 100 nm appear at the peak region of helium-implanted nickel after annealing at 500 °C for 2 h.[24] The fluence was 5×10^{17} ions/cm^2 and other irradiation conditions were nearly the same as our present study. However, the average size of bubbles at the peak region of alloy 617 is 13 nm, much less than that in nickel, suggesting the better helium irradiation resistance of alloy 617. This discrepancy should be attributed to the sluggish migration of the helium bubble in alloy 617. The atomic sizes of the main alloying elements in alloy 617 are larger than that of Ni, such as Co, Cr, and Mo, which lead to a smaller surface diffusivity.[25] The bubbles migrate through the diffusion of matrix atoms on the surface, which causes the random rearrangements of other matrix atoms.[26] Hence, compared to pure nickel, the migration and coalescence of bubbles are suppressed in alloy 617.

4. Conclusion and perspectives

The nickel-based alloy 617 was irradiated then post-implantation annealed, and the helium bubbles evolution with post-implantation annealing and their related mechanism have been investigated by TEM. Many over-pressurized and small helium bubbles formed during the room temperature implantation are observed. Bubble coarsening upon annealing at 700 °C is observed with the bubble shape variation in different regions. The helium bubbles are spherical at a depth less than 400 nm or deeper than 750 nm. while at the depth of 400 nm–750 nm, the helium bubbles are faceted in shape to minimize the system energy. The long-range migration of helium bubbles occurred during the annealing process and the coarsening of helium bubbles at different depths is through the MC mechanism. Therefore, it may help the helium distribution and evolution behavior of helium–vacancy clusters, further evaluating and predicting the irradiation resistance properties.

References

[1] Abram T and Ion S 2008 *Energy Policy* **36** 4323
[2] Locatelli G, Mancini M and Todeschini N 2013 *Energy Policy* **61** 1503
[3] Forsberg C W, Peterson P F and Pickard P S 2003 *Nucl. Technol.* **144** 289
[4] Ren W and Swindeman R 2009 *Journal of Pressure Vessel Technology* **131** 044002
[5] Sharma S K, Ko G D, Li F X and Kang K J 2008 *J. Nucl. Mater.* **378** 144
[6] Wolfer W 2012 *Fundamental properties of defects in metals*
[7] Trinkaus H and Singh B 2003 *J. Nucl. Mater.* **323** 229
[8] Schroeder H, Kesternich W and Ullmaier H 1985 *Nuclear Engineering and Design: Fusion* **2** 65
[9] Ullmaier H 1984 *Nuclear Fusion* **24** 1039
[10] Singh B and Trinkaus H 1992 *J. Nucl. Mater.* **186** 153
[11] Greenwood G, Foreman A and Rimmer D 1959 *J. Nucl. Mater.* **1** 305
[12] Carsughi F, Ullmaier H, Trinkaus H, Kesternich W and Zell V 1994 *J. Nucl. Mater.* **212** 336
[13] Villacampa I, Chen J, Spätig P, Seifert H and Duval F 2018 *J. Nucl. Mater.* **500** 389
[14] Chen Y, Li Y, Ran G, Wu L, Ye C, Han Q, Wang H and Du H 2020 *Prog. Nucl. Energy* **129** 103502
[15] Ziegler J F, Ziegler M D and Biersack J P 2010 *Nucl. Instrum. Methods Phys. Res. Sect. B: Beam Interactions with Materials and Atoms* **268** 1818
[16] Lv S, Zhu R, Zhao Y, Li M, Wang G, Qiu M, Liao B, Hua Q, Cheng J and Li Z 2020 *Chin. Phys. B* **29** 040704
[17] Zhang Y, Lian J, Zhu Z, Bennett W D, Saraf L V, Rausch J L, Hendricks C A, Ewing R and Weber W J 2009 *J. Nucl. Mater.* **389** 303
[18] Goodhew P 1981 *The shape of an overpressurized bubble*
[19] Chernikov V, Trinkaus H, Jung P and Ullmaier H 1990 *J. Nucl. Mater.* **170** 31
[20] Trinkaus H 1989 *Scripta Metallurgica* **23** 1773
[21] Chernikov V, Trinkaus H and Ullmaier H 1997 *J. Nucl. Mater.* **250** 103
[22] Wei Q, Nan L, Kai S and Wang L M 2010 *Scripta Materialia* **63** 430
[23] Gao J, Bao L, Huang H, Li Y, Zeng J, Liu Z, Liu R and Shi L 2016 *Materials* **9** 832
[24] Yan Z, Liu S, Xia S, Zhang Y, Wang Y and Yang T 2018 *J. Nucl. Mater.* **505** 200
[25] Liu J, Huang H, Liu R, Zhu Z, Lei Q, Liu A and Li Y 2020 *J. Nucl. Mater.* **537** 152184
[26] Zhang W, Han H, Dai J, Ren C, Wang C, Yan L, Huang H and Zhu Z 2019 *J. Nucl. Mater.* **518** 48